AIAA JOURNAL
Vol. 35, No. 4, April 1997

Numerical Algorithms for Acoustic Integrals with Examples for Rotor Noise Prediction

Kenneth S. Brentner*
NASA Langley Research Center, Hampton, Virginia 23681-0001

The accurate prediction of the aeroacoustic field generated by aerospace vehicles or nonaerospace machinery is necessary for designers to control and reduce source noise. Powerful computational aeroacoustic methods, based on various acoustic analogies (primarily the Lighthill acoustic analogy) and Kirchhoff methods, have been developed for prediction of noise from complicated sources, such as rotating blades. Both methods ultimately predict the noise through numerical evaluation of an integral formulation. We consider three generic acoustic formulations and several numerical algorithms that have been used to compute the solutions to these formulations. Algorithms for retarded-time formulations are the most efficient and robust, but they are difficult to implement for supersonic-source motion. Collapsing-sphere and emission-surface formulations are good alternatives when supersonic-source motion is present, but the numerical implementations of these formulations are more computationally demanding. New algorithms—which utilize solution adaptation to provide a specified error level—are needed.

Nomenclature

c	= sound speed in undisturbed medium
dS	= element of source surface
$d\Sigma$	= element of emission (influence) surface
$d\Omega$	= element of collapsing-sphere surface
$F = 0$	= function that describes the emission surface, $F(\boldsymbol{y}, \boldsymbol{x}, t) = [f(\boldsymbol{y}, \tau)]_{\text{ret}} = f(\boldsymbol{y}, t - r/c)$
$f = 0$	= function that describes the source surface
$g = 0$	= surface that describes the collapsing sphere, $g = \tau - t + r/c$
$H(f)$	= Heaviside function
M_r	= Mach number of the source in the radiation direction
$\hat{\boldsymbol{n}}$	= unit outward normal vector to surface
p'	= acoustic pressure
r	= distance between observer and source, $r = \lvert\boldsymbol{x} - \boldsymbol{y}\rvert$
$\hat{\boldsymbol{r}}$	= unit vector in the radiation direction, $(\boldsymbol{x} - \boldsymbol{y})/\lvert\boldsymbol{x} - \boldsymbol{y}\rvert$
t	= observer time
v_n	= local normal velocity of source surface
$\boldsymbol{x}$	= observer position
$\boldsymbol{y}$	= source position
$\Gamma = 0$	= intersection of collapsing sphere and source surface
γ	= angle used to measure circular arc (see Fig. 4)
$\delta(f)$	= Dirac delta function
θ	= angle between $\hat{\boldsymbol{n}}$ and $\hat{\boldsymbol{r}}$
Λ	= $\sqrt{(1 - 2M_n \cos\theta + M_n^2)}$
ρ_0	= density in undisturbed medium
τ	= source time
$\Box^2$	= wave operator, d'Alembertian

Subscript

ret	= quantity is evaluated at the retarded time, $\tau = t - r/c$

Introduction

A GREAT deal of progress has been made in recent years toward prediction of rotor noise through the utilization of first-principles methods. Several reasons account for this progress. First, a detailed and fundamental understanding of how rotor blades generate noise has been gained through a series of acoustic wind-tunnel and flight tests. Second, a rigorous theoretical basis of noise generated by rotating blades was introduced in 1969 by Ffowcs Williams and Hawkings.[1] The Ffowcs Williams–Hawkings (FW–H) equation is an extension of the Lighthill acoustic analogy to sound generated by surfaces in arbitrary motion and is the starting point for most rotor noise prediction. Because the FW–H equation is an exact rearrangement of the continuity and Navier–Stokes equations into the form of an inhomogeneous wave equation, in principle, the solution to the FW–H equation will also be exact if the input data are exact.

In practice, however, the veracity of the input data and the numerical approach both play major roles in determining the accuracy of the acoustic prediction. In a recent paper by Gallman et al.,[2] several helicopter rotor noise prediction codes were given identical input data to predict blade–vortex interaction (BVI) noise for a model helicopter rotor. Although the codes were numerical implementations of the same formulation of the FW–H equation, the codes gave significantly different answers for several of the operating conditions and observer locations considered. These differences ranged from some codes not even predicting BVI noise in one case to BVI pulse amplitudes varying significantly. Directivity patterns were similar for all of the codes, but peak predicted noise varied by as much as 3–4 dB between codes. This seems highly undesirable when we recall that the same input data and formulation were used by all the codes. Although the discrepancies have not been explained, a detailed comparison of each of the numerical implementations is clearly needed to determine the reason for the discrepancies. The study by Gallman et al. illustrates that the discipline of computational acoustics is becoming more discerning—an assessment of solution accuracy is also needed along with the acoustic prediction.

This paper focuses on the various choices that can be made both in the selection of formulation and in the numerical implementation of acoustic integrals and discusses how these choices affect the accuracy and robustness of the acoustic predictions. These details are at the heart of every prediction code, yet they rarely receive sufficient attention in the literature. The bias of this paper is toward external flow problems—in particular, rotor noise. Because of the predominance of time-domain formulations in rotor noise prediction, only time-domain formulations are considered in this paper. This paper is an attempt to stimulate thought on the numerical aspects of acoustic codes based on the acoustic analogy and Kirchhoff formulations. Ultimately, this consideration and scrutiny should help to improve the accuracy, efficiency, and robustness of integral-based acoustic predictions.

Presented as Paper 96-1706 at the AIAA/CEAS 2nd Aeroacoustics Conference, State College, PA, May 6–8, 1996; received June 24, 1996; revision received Dec. 30, 1996; accepted for publication Jan. 21, 1997.

*Research Engineer, Aerodynamic and Acoustic Methods Branch, Fluid Mechanics and Acoustics Division. Senior Member AIAA.

Formulation vs Numerical Algorithm

The FW–H equation and its close relative, the Kirchhoff formulation, are usually formulated through use of a Green's function. In the case of the rotating blade noise, the free-space Green's function $\delta(g)/4\pi r$ leads to an integral representation of the solution. We use the term integral representation because the integral formulation must either be solved as a singular integral equation or, as is most often done in rotor noise prediction, the flowfield data in the source region must be given as input to determine the acoustic solution outside the source region. The particular formulation that is developed results primarily from the choice of the change of variables needed to analytically integrate the Dirac delta functions.

To illustrate this explanation, we consider the following example. An inhomogeneous wave equation can be written as

$$\Box^2 \phi(\boldsymbol{x}, t) = Q(\boldsymbol{x}, t)\delta(f) \tag{1}$$

where $Q(\boldsymbol{x}, t)$ is the source strength and $f(\boldsymbol{x}, t) = 0$ defines a surface over which the source is distributed. Equation (1) is typical of the various source terms in the FW–H equation. By using the free-space Green's function $\delta(g)/4\pi r$, an integral representation of the solution may be written as

$$4\pi\phi(\boldsymbol{x}, t) = \int_{-\infty}^{t}\int_{-\infty}^{\infty} \frac{Q(\boldsymbol{y}, \tau)\delta(f)\delta(g)}{r}\,\mathrm{d}\boldsymbol{y}\mathrm{d}\tau \tag{2}$$

The next stage in developing the acoustic formulation is to integrate the Dirac delta functions $\delta(f)$ and $\delta(g)$, a process that requires a change of variables. The change of variables determines the type of formulation. Equation (2) can be expressed as

$$4\pi\phi(\boldsymbol{x}, t) = \int_{f=0} \left[\frac{Q(\boldsymbol{y}, \tau)}{r|1 - M_r|}\right]_{\text{ret}} \mathrm{d}S \tag{3}$$

$$= \int_{-\infty}^{t}\int_{\substack{f=0\\g=0}} \frac{Q(\boldsymbol{y}, \tau)}{r\sin\theta}\, c\,\mathrm{d}\Gamma\mathrm{d}\tau \tag{4}$$

$$= \int_{F=0} \frac{1}{r}\left[\frac{Q(\boldsymbol{y}, \tau)}{\Lambda}\right]_{\text{ret}} \mathrm{d}\Sigma \tag{5}$$

with the variable transformations $(\tau, y_3) \longrightarrow (g, f)$, $(y_2, y_3) \longrightarrow (f, g)$, and $(\tau, y_3) \longrightarrow (g, F)$, respectively (see Ref. 3). The three formulations expressed in Eqs. (3–5) are termed retarded-time, collapsing-sphere, and emission-surface formulations, respectively. Time-domain acoustic formulations can be classified as one of these generic types; each type has its own physical and geometrical interpretation. These formulations and their interpretations are discussed in the next section. If the source in Eq. (1) had been a volume distribution, analogous integral formulas would result. (Reference 4 discusses many of the specific linear formulations used in rotating blade noise prediction.)

The numerical algorithm, on the other hand, has to do with the numerical procedure and the approximations required to provide a discrete result from the analytical formulation. The formulation provides the framework and geometrical interpretation; we use the term algorithm to refer to how the integral is numerically evaluated. The accuracy, efficiency, and robustness of the numerical algorithm depend strongly on the choice of both the formulation and the algorithm, yet the details of the numerical implementation can significantly affect code performance. For example, high-order integration and adaptive quadrature algorithms can potentially be much more accurate and efficient than simpler counterparts for the same formulation. A detailed comparison of the formulations and the related algorithms is presented in the remainder of the paper.

Numerical Algorithms

Numerical algorithms vary significantly among different formulation types, even though the same physical and mathematical problem is ultimately solved. For this reason, the algorithms discussed in this paper are categorized by the type of formulation with which they are associated. In this section, the three different types of formulations are treated separately. A brief description and a geometrical interpretation are given, followed by a more detailed discussion of the algorithm and its application for each formulation. The discussion in this section is restricted to algorithms for surface-source distributions, but analogous techniques are available for integration of volume-source distributions.

Retarded-Time Algorithms

We first consider the retarded-time formulation

$$4\pi\phi(\boldsymbol{x}, t) = \int_{f=0} \left[\frac{Q(\boldsymbol{y}, \tau)}{r|1 - M_r|}\right]_{\text{ret}} \mathrm{d}S \tag{6}$$

where Q is the known source strength, which is a function of the source position and time $(\boldsymbol{y}, \tau)$. Normally in acoustic predictions, ϕ is the acoustic pressure p'. The interpretation of Eq. (6) is that integration occurs over the physical surface, with the integrand evaluated at the emission, or retarded, time $\tau* = t - r/c$. The integration is easy to understand because the integration surface is given as part of the source description. Note that the formulation requires that the observer location $\boldsymbol{x}$ and the observer time t are fixed during the evaluation of the integral. Numerical implementations of this formula have proven to be very robust and efficient; hence, most acoustic analogy-based rotor noise predictions (e.g., Refs. 5–11) and Kirchhoff codes (e.g., Refs. 12–16) utilize retarded-time formulations.

Midpanel Quadrature

The most common method of numerically evaluating retarded-time integrals is to approximate the integral as follows:

$$4\pi\phi(\boldsymbol{x}, t) \approx \sum_{i}^{N}\left[\frac{Q(\boldsymbol{y}_i, t - r_i/c)}{r_i|1 - M_r|_i}\right]_{\text{ret}} \Delta S_i \tag{7}$$

Here, the surface S is divided into N panels, and the integrand is evaluated at the center of each panel $(\boldsymbol{y}_i)$ at that point's retarded time. If the source is not moving, then the determination of the retarded time $\tau*$ is made by a simple computation $\tau* = t - r_i/c$, where $r_i = |\boldsymbol{x} - \boldsymbol{y}_i|$. If the source is in motion, then the source position is a function of the retarded time [i.e., the desired $\boldsymbol{y}_i$ is $\boldsymbol{y}_i(\tau*)$] and, unless the source motion is simple, the retarded time cannot practically be determined analytically. The retarded time, then, is found numerically as the root of the equation $t - \tau - r(\tau)/c = 0$. Even when the source motion is complex, such as for a helicopter main rotor, standard root-finding algorithms work well (e.g., see Ref. 17). Because the source strength Q is evaluated at the retarded time, temporal interpolation of the input data is usually required. A time history of ϕ is developed by choosing both the observer position and the observer time, evaluating the summation in Eq. (7), and then choosing the next observer time in the time history. Equations (6) and (7) can be used to find the time history of ϕ for a moving observer if the observer position is moved for each evaluation of the integral.

The approximation given in Eq. (7) with $\boldsymbol{y}_i$ at panel centers is in widespread use and works well as long as the panel size is sufficiently small. In this case, sufficiently small means that the source strength variation is approximately linear over the panel and the retarded time does not vary significantly over the panel (i.e., $\Delta\tau \ll$ typical period of fluctuations). Refinement of the panel size is clearly needed if the source strength Q is not linear over the panel because Q is not resolved and the midpoint value is unlikely to represent the mean value. Insufficient resolution of the source strength can occur in practice whenever the noise source is physically localized, such as occurs in blade–vortex interaction noise for helicopter rotors; therefore, we must require that the input data resolve the source spatially and temporally.

A subtle but extremely important point is that the variation of Q over a panel in retarded-time space can be much more significant than the variation of Q over a panel at single source time. Meadows and Atkins[15] noticed this phenomenon in a Kirchhoff computation of noise generated by an oscillating sphere. They used high-order interpolation and quadrature but found that more points per wavelength

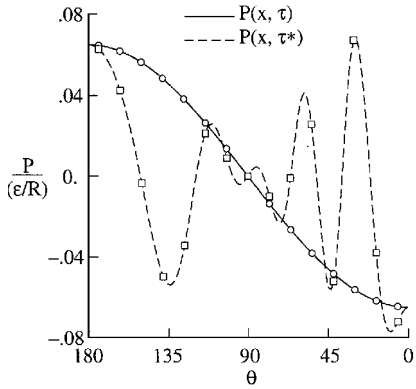

Fig. 1 Pressure at one source time τ compared with pressure evaluated at retarded time $\tau*$ for Kirchhoff calculation by Meadows and Atkins.[15]

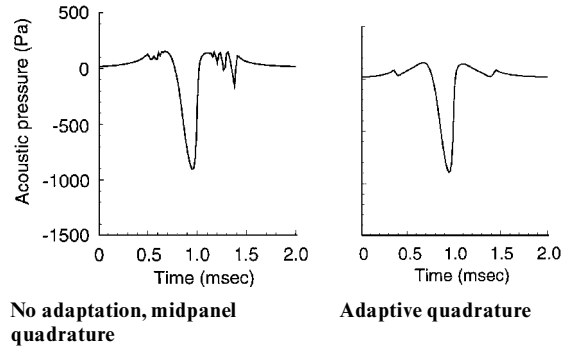

Fig. 2 Comparison of predicted solution with and without an adaptive quadrature algorithm. (Note that considerable panel size variation occurred in this computation.)

than expected were needed on the Kirchhoff surface to achieve the desired accuracy. Figure 1 (from Ref. 15) compares the pressure on the integration surface at one source time τ to the pressure as a function of retarded time $\tau*$.

Although the pressure plotted in Fig. 1 is not over one panel but over one meridian line on the spherical Kirchhoff surface, the idea is the same—the function behavior in retarded-time space can be significantly different from that at any individual source time. A large panel size with certain observer orientations ($\hat{\boldsymbol{n}}\ \hat{\boldsymbol{r}} \longrightarrow 0$) and a large panel velocity ($M_r \longrightarrow 1$) can both lead to large variations in retarded time over a panel. Kirchhoff methods are likely to have both larger panels and significant retarded-time variation over a panel, because the Kirchhoff integration surface is located some distance from the physical source region and must surround it.

High-Accuracy Quadrature

A refinement of Eq. (7) can be made by replacing the single evaluation of the integrand at the panel center with more points; thus, greater accuracy is achieved. The discrete computation would then be

$$4\pi\phi(\mathbf{x}, t) \approx \sum_{i}^{N}\left(\sum_{j}^{n_i}\alpha_j\left[\frac{Q(\mathbf{y}_j, t - r_j/c)}{r_j|1 - M_r|}\right]_{\text{ret}}|J|_j\right)\Delta S_i \qquad (8)$$

where α_j and $|J|_j$ are the quadrature weight coefficient and determinant of the Jacobian of the transformation, respectively, for the jth point in the panel quadrature algorithm. The weights α_j and the location of the quadrature points $\mathbf{y}_j$ can be chosen to increase the order of polynominal approximation used for the panel quadrature. Thus, with a larger number of points the limitations of the mid-panel algorithm can be overcome. Farassat et al.[18] and Dunn and Tarkenton[19] utilize a high-order quadrature algorithm of this type in their propeller noise prediction code ASSPIN.

The full benefit of a high-accuracy quadrature is realized, however, when a solution-adaptive quadrature scheme is utilized. This feature is included in Eq. (8) by selecting the number of quadrature points n used in the ith panel with some parameter related to the solution; that is, a larger number of quadrature points are used only when the function variation over the panel requires it. An adaptive-quadrature scheme can provide high accuracy and minimize the computational effort. Brentner and Holland[10] developed an adaptive-quadrature algorithm in a far-field quadrupole noise prediction. Their adaptation parameter was

$$n_i(M_r, \Delta S_i) \propto \frac{\Delta S_i}{|1 - M_r|} \qquad (9)$$

where M_r (the Mach number of the panel center in the radiation direction) and ΔS_i (the physical area of the panel) were used to determine the number of Gauss–Legendre quadrature points in the chordwise direction of the panel; n_i is scaled so that $1 \leq n_i \leq 20$. As M_r approaches unity or if the area of the panel is large, the adaptation parameter becomes large. Similarly, if M_r is small or the area of the panel is small, then the adaptation parameter becomes small. The computation with adaptive quadrature required little additional computer time but yielded a significantly better signal, as shown in Fig. 2. (Note that the two remaining bumps at times $t = 0.4$ and 1.5 are an artifact of the chordwise truncation of the quadrupole source integration region ahead and behind the blade. Each quadrupole panel has a contribution—because of the entropy generated by the shock—that is normally canceled for panels away from the rotor by the adjacent panels. The proper cancelation does not occur in the figure because the integration domain is truncated.) Although the adaptive quadrature of Brentner and Holland[10] worked well in their application, what is really needed is an adaptive quadrature scheme that is based on a measure of error in the solution.

Consider again the spatial (θ) resolution of source pressure for a single source time τ in Fig. 1. In that case, as is generally necessary if we have any hope of predicting the acoustics, the source is well-resolved both spatially and temporally. Only the acoustic quadrature may need additional spatial information to achieve the desired accuracy. Hence, in Eq. (8) the source strength Q is expediently evaluated at the $\mathbf{y}_j$ quadrature points by a spatial interpolation of Q at the fixed source time $\tau*$. The procedure for this evaluation is 1) determine the retarded time τ_j* for the quadrature point $\mathbf{y}_j$; 2) perform a temporal interpolation of the data to the retarded time τ_j* at each spatial location in the input data needed for the spatial interpolation; and 3) perform the spatial interpolation of $Q(\mathbf{y}, \tau_j*)$ to the point $\mathbf{y}_j$. Brentner and Holland[10] used linear interpolation for both the temporal and spatial interpolations in this adaptive quadrature algorithm. Meadows and Atkins[15] called the procedure of spatial interpolation at constant source time "enrichment" to emphasize that the computational fluid dynamics (CFD) solution, which is the most expensive part of the calculation, was not refined.

Source Time-Dominant Algorithm

A completely different approach can be taken to evaluate a retarded-time integral if source time is regarded as dominant. Rather than select the observer time in advance, one can now choose the source time for a panel (by again using the panel center) and determine when the signal will reach the observer. If the observer $\boldsymbol{x}$ is stationary, then $t = \tau + r_i/c$; otherwise, we must find the root of the equation $t - \tau - |\mathbf{x}(t) - \mathbf{y}_i(\tau)|/c = 0$. The determination of t even for the latter case is easier than finding the retarded time, because observer motion is usually simple; hence, the solution for t can be found analytically. A sequence of source times (e.g., the times at which the source strength is available) will lead to a sequence of unequally spaced observer times. This panel time history can be interpolated to provide the contribution at the desired observer times. Interpolation in time is necessary so that the contributions from all source panels can be added together at the same observer times. This algorithm can be written symbolically as

$$4\pi\phi(\mathbf{x}, t*) \approx \sum_{i}^{N} I[K_i(t), t*] \qquad (10)$$

where $I(\ , t*)$ is an interpolation operator and $t*$ is the desired observer time. The approximation of the integral over the panel K is defined as

$$K_i(t) = \frac{Q(\mathbf{y}_i, \tau)}{r_i|1 - M_r|_i}\Delta S_i \qquad (11)$$

The value of $t*$ is determined by the selection of $\boldsymbol{y}_i$ and τ. This algorithm has the advantage that a retarded-time calculation is not necessary per se and the discrete time-dependent input data do not need to be interpolated. This characteristic may be useful when a CFD code provides the input data. Another computational advantage of the source time-dominant algorithm is that the solution process is inherently parallel; thus, the algorithm is a good candidate for parallel computers. Nevertheless, we do not yet know how a source time-dominant algorithm can be made solution adaptive or how the computation time and accuracy will compare with the observer time-dominant algorithm. Xue has implemented this algorithm in a general Kirchhoff aeroacoustics code.[20]

Supersonic-Source Motion

Although retarded-time algorithms are robust, they have one drawback—for supersonic-source motion the integrals become singular (i.e., when $M_r = 1$ the Doppler factor $|1 - M_r| = 0$) and the retarded-time equation can have multiple roots. The multiple roots for supersonic-source motion can be found without too much trouble, but the real problem is the Doppler singularity in the integrand. The necessary regularization of the integral requires both mathematical analysis and conditional code logic. As an alternative, either the collapsing-sphere method or the emission-surface method may be used to avoid the singularity. In Refs. 18 and 19, the formulation is switched for supersonic panels to realize the efficiency and robustness of the retarded-time formulation for subsonic panels while enabling the code to handle supersonic-source motion. (Note that the source velocity is the velocity of the source point rather than the fluid velocity. Also, the Mach number M_r is based on the sound speed of the undisturbed medium rather than the local sound speed of the fluid.)

Collapsing-Sphere Algorithms

Now we turn our attention to the collapsing-sphere formulation

$$4\pi\phi(\boldsymbol{x}, t) = \int_{-\infty}^{t} \int_{\substack{f=0 \\ g=0}} \frac{Q(\boldsymbol{y}, \tau)}{r \sin\theta} c \, \mathrm{d}\Gamma \, \mathrm{d}\tau \tag{12}$$

In Eq. (12), the inner integration is over the intersection of the source surface $f = 0$ and the surface defined by $g = \tau - t + r/c = 0$. The equation $g = 0$ (which is exactly the retarded-time relationship) can be interpreted as the equation of a sphere with radius r centered at the observer position $\boldsymbol{x}$ for a particular source time τ. Recall that the observer position and time $(\boldsymbol{x}, t)$ are fixed during the integration in Eq. (12); hence, as τ approaches t the radius of the sphere reduces or collapses. The collapsing sphere contains all points in space that can potentially emit, at source time τ, a signal that will be received by the observer $\boldsymbol{x}$ at time t; the intersection of $g = 0$ and $f = 0$ (called a Γ curve) is the collection of source points that do emit a signal at source time τ that reaches the observer at time t. A schematic is shown in Fig. 3. The collapsing-sphere formulation does not have a Doppler singularity; however, this formulation does have a singularity in the integrand that occurs when the surface normal vector $\hat{\boldsymbol{n}}$ is parallel to the radiation vector $\hat{\boldsymbol{r}}$ (i.e., $\sin\theta = 0$).

Farassat and Brown[21] were the first to develop a collapsing-sphere algorithm to predict the noise from thickness and loading source terms of the FW–H equation. They computed thickness and loading noise for a moving, noncompact source with realistic source geometry for both subsonic- and supersonic-source motion. In their code, Farassat and Brown evaluated the double integrals numerically with the following algorithm:

1) Determine the initial observer time t_i for which the collapsing sphere intersects the source surface.

2) Choose the value of τ_j.

3) Determine the intersection of the collapsing sphere $g = 0$ and the source surface $f = 0$. The Γ curve is approximated by straight line segments.

4) Compute the integrands at the ends of the line segments and evaluate the line integral over the Γ curve by trapezoidal rule.

5) Advance the source time τ_j and repeat 3 and 4 until the collapsing sphere no longer intersects the source surface. Compute the τ integration with Simpson's rule.

6) Repeat this process for each observer time in the time history.

This algorithm is computationally demanding because a construction of the Γ curves must be done many times for each observer time. Experience has shown that the collapsing-sphere algorithm outlined here requires 1 to 2 orders of magnitude more computer time than the midpanel quadrature retarded-time algorithm. The retarded-time algorithm is much faster because the retarded time $\tau*$ must be found only once per source panel for each observer time. Another problem experienced by Farassat and Brown was that the computed solution was oscillatory and required numerical smoothing. The $\sin\theta$ term in the denominator of Eq. (12) must be at least partially responsible for the numerical oscillations.

The collapsing-sphere formulation has not been widely used in practice; however, with new numerical algorithms this formulation may prove to have some advantages. For example, if the source surface is approximated as a set of planar panels, then the intersection of the collapsing sphere and the panel is a circular arc with its center at $\boldsymbol{X0} = \boldsymbol{x} + r\cos\theta\hat{\boldsymbol{n}}$. The radius of the circular arc is $r\sin\theta$. The geometry of the collapsing-sphere intersection with a planar panel is shown in Fig. 4. On the basis of this geometry, we see that $\mathrm{d}\Gamma = r\sin\theta\,\mathrm{d}\gamma$ and Eq. (12) may be written

$$4\pi\phi(\boldsymbol{x}, t) = \int_{-\infty}^{t} \int_{\Delta\gamma} Q(\boldsymbol{y}, \tau) c \, \mathrm{d}\gamma \, \mathrm{d}\tau \tag{13}$$

for a single panel. The notation $\Delta\gamma$ implies that Q is evaluated on the portion of the Γ curve that lies on the panel. The result in Eq. (13) has not been used in application but is interesting because the $r\sin\theta$ term in the denominator is absent; hence, the integral is quite simple, and the quadrature is likely to be robust. Also, the number of quadrature points in the γ quadrature can easily be selected to improve the accuracy. We do not know, however, whether the planar panel assumption will be appropriate in general, but for some special cases (e.g., the far-field quadrupole approximation used by Brentner and Holland[10]) the source panels are planar. [Note that when $\sin\theta = 0$ the contribution of the inner integral in Eq. (13) comes from a single point.]

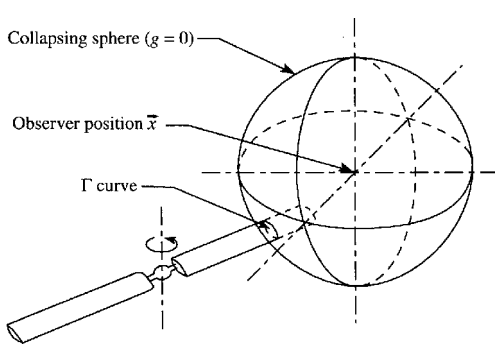

Fig. 3 Schematic of collapsing sphere that intersects rotor blade.

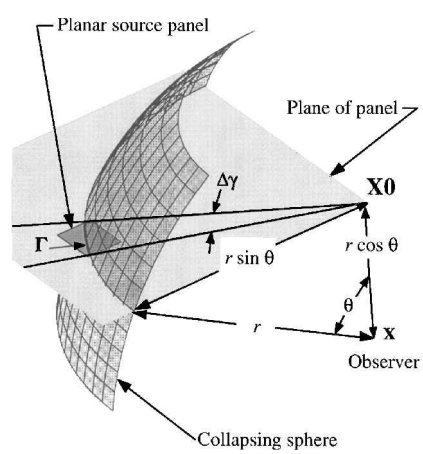

Fig. 4 Schematic of collapsing-sphere intersection with single planar source panel.

Emission-Surface Algorithms

Finally, we consider the general form of an emission-surface formulation:

$$4\pi\phi(\mathbf{x}, t) = \int_{F=0} \frac{1}{r}\left[\frac{Q(y, \tau)}{\Lambda}\right]_{\text{ret}} \mathrm{d}\Sigma \qquad (14)$$

where the Σ surface is the emission, or influence, surface. The Σ surface is the collection of points in space time that emits signals that reach the observer at one particular observer time. The emission surface is sometimes referred to as the acoustic planform, but we reserve this terminology for when we mean the projection of the Σ surface onto a thin surface [i.e., the helicoidal surface swept out by a propeller (e.g., see Ref. 22) or the rotor disk for a helicopter rotor]. The Σ-surface formulation does not suffer from the Doppler singularity, but a true singularity can occur when the surface normal vector $\hat{\boldsymbol{n}}$ of a source point is parallel to the radiation vector $\hat{\boldsymbol{r}}$ and the source point is moving toward the observer at exactly sonic speed (i.e., $\Lambda = 0$). This singularity is an indication of a caustic in the solution; Farassat and Myers[23] have shown for the FW–H equation that the singularity from the surface source is eliminated if the quadrupole-source term is included.

The main difficulty in the numerical evaluation of Eq. (14) is construction of the Σ surface. The Σ surface can be constructed by using either a retarded-time computation to determine the location of the source points at the retarded time or through the process of computing the intersection of the collapsing sphere with the source surface. Special care must be taken in the construction, because the Σ surface may be composed of several disjoint pieces when the source motion is supersonic; this situation is exactly the type of situation that could lead to use of the emission-surface formulation.

Brentner[24] has developed an alternative method for constructing the Σ surface and performing the integration in Eq. (14) based on a computer graphics algorithm. The approach is similar to the source time-dominant algorithm presented in the retarded-time algorithms section; the source time is chosen and the corresponding observer time is computed at each grid point. If the observer times are computed and stored for each desired source time, the discrete computational data become a three-dimensional array; indices i and j parameterize the surface spatially and index k accounts for the source time. In this three-dimensional computational space, isosurfaces of observer time t are, by definition, distinct realizations of the Σ surface. The problem of constructing the Σ surface is equivalent to the construction of isosurfaces, which is an important problem in computer graphics.

Surface reconstruction must be done very efficiently and quickly to be useful for interactive data visualization. Lorensen and Cline[25] have developed the method of marching cubes, which uses a two-step approach to the surface-construction problem. The first step is to locate the surface that corresponds to the level desired and approximate it with triangles. The second step is to calculate a surface normal vector at each triangle vertex. The marching-cubes method uses a divide-and-conquer approach to locate the surface in a logical cube created from eight data points (four each from two adjacent layers, as shown schematically in Fig. 5).

The extension of the marching-cubes algorithm for surface integration[24] determines how the surface intersects the cube, computes the contribution to the integral from that portion of the surface, and then moves (or marches) to the next cube. The topology of the surface can be determined uniquely by examining the function value (observer time in this case) at each of the cube vertices and comparing this value to the desired surface value. A table lookup is then used to determine the exact topology of the surface in the current cube. The surface is formed by a set of triangular panels that have vertices on the edges of the cubes. Brentner[24] took the value of the surface integral over each triangle as the average integrand value of the triangle vertices multiplied by the triangle area. Linear interpolation is used to determine the integrand values at the triangle vertices based on the previously computed value at the cube vertices. (For more detail on the marching cubes algorithm, see Refs. 24 and 25.)

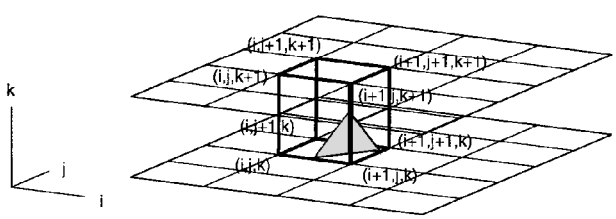

Fig. 5 Schematic of logical grid, marching cube, and triangular piece of surface in marching cube.

Because computations in the marching-cubes integration algorithm are done locally, one cube at a time, the computational problem can be easily separated into blocks. This separation minimizes the necessary computer storage requirements. Computation locality should also make the marching-cubes integration algorithm a good candidate for parallel computer architectures. Another advantage of the marching-cubes integration algorithm is that the methodology is not closely coupled to the physical problem; hence, the integration routine can be readily applied to a large class of problems. The marching-cubes algorithm has no particular problem in finding surfaces that are disjoint, which is an important attribute in considering algorithms for use with supersonically moving sources. The numerical integration is accurate only to low order. Improvements in accuracy may be possible by using higher-order interpolation and panel geometries other than flat triangles, but some simplicity and locality would be compromised in the process.

Solution Adaptive Algorithms

Although a brief discussion of solution adaptation was given in the discussion of high-accuracy quadrature in the retarded-time algorithms section, this subject is important enough that we need to consider it again here. Solution adaptation is usually done to improve solution accuracy or to reduce computational time. The ideal numerical algorithm for each formulation would be adaptive for both reasons. Two types of solution adaptation are recommended here.

Temporal Adaptation

In rotor noise prediction, the acoustic signal generally consists of a local pulse preceded and followed by periods without significant acoustic pressure fluctuations. Although most current codes divide the time history in equally spaced increments of time, this approach is not the most computationally efficient. Variation of the time-step size can reduce the total computational work by minimizing the number of points needed to resolve the signal, but it will not improve the quadrature accuracy at any particular observer time. In the rotor noise prediction code PARIS,[7] the time steps are chosen in an unequal manner with a concentration of time steps within the main acoustic pulse. By using a variable time step, the computation time is reduced by more than 1 order of magnitude. The propeller code ASSPIN[20] also uses variable time steps. Fine time steps are taken when the panel is moving supersonically (the acoustic signal has steep gradients when the blade is moving supersonically), and coarse time steps are taken when the panel is moving subsonically.

One way to minimize the number of time steps in the acoustic computation is to dynamically choose the discrete observer time steps. This selection can be done by computing the acoustic solution at several large, equally spaced times and then refining the solution by clustering time points at locations where the second time derivative of $\phi(\mathbf{x}, t)$ is large. Furthermore, a minimum time step size or maximum number of allowable points should also be specified.

Quadrature Adaptation

We refer to another type of solution adaptation as "quadrature adaptation." In quadrature adaptation, the number and location of the quadrature points, in space or time, can be selected to increase the accuracy of the quadrature. Several codes have utilized some sort of refinement to improve the solution accuracy (e.g., see Refs. 10, 15, 19, and 26); however, none of these algorithms monitors the error of the solution. Without a measure of the error, the algorithm cannot determine whether a sufficient number of quadrature points have been used to achieve the desired accuracy or whether too many points are being used; this approach is inefficient.

Perhaps we should examine the procedure used by advanced ordinary differential equation (ODE) solvers. These ODE solver

algorithms are relevant because integration can always be recast into the form of a differential equation. An efficient ODE solver takes large steps in regions in which the function varies slowly and small steps in treacherous regions in which the function varies rapidly. To determine the approximate solution error, the solver might take a large step followed by two smaller steps over the same interval and then compare the results. The algorithm adjusts the step size dynamically to ensure that the solution meets the specified error criteria. (See Ref. 17 for more discussion on adaptive step-size ODE solver algorithms.) If this type of algorithm were applied to the numerical integration of acoustic integrals, the user would be assured of the solution accuracy. The work required by adaptive ODE algorithms is often orders of magnitude less than for constant step-size algorithms because these algorithms can take large steps when appropriate. For this reason, we propose that this technology should be incorporated into future acoustic-integral algorithms.

Summary

We have discussed several of the numerical algorithms available for solution of acoustic integrals. The presentation of these algorithms is applicable to formulations that originate from either an acoustic analogy or a Kirchhoff method. The type of formulation (retarded time, collapsing sphere, or emission surface) determines, to a large extent, the ultimate computational efficiency and robustness of the algorithm, but several implementation options exist for each formulation. Retarded-time algorithms are the most robust and efficient type, but retarded-time algorithms are not well-suited to applications with supersonic-source motion. Solution adaptation has been demonstrated to increase accuracy and reduce computational work. Future solution adaptation should utilize a measure of the solution error in the adaptation process.

References

[1]Ffowcs Williams, J. E., and Hawkings, D. L., "Sound Generated by Turbulence and Surfaces in Arbitrary Motion," *Philosophical Transactions of the Royal Society*, Vol. A264, No. 1151, 1969, pp. 321–342.

[2]Gallman, J. M., Tung, C., Schultz, K. J., Splettstoesser, W., Buchholz, H., Spiegel, P., Burley, C. L., Brooks, T. F., and Boyd, D., Jr., "Effect of Wake Structure on Blade–Vortex Interaction Phenomena: Acoustic Prediction and Validation," CEAS/AIAA Paper 95-051, June 1995.

[3]Farassat, F., "Theory of Noise Generation from Moving Bodies with Application to Helicopter Rotors," NASA TR-451, Dec. 1975.

[4]Farassat, F., "Linear Acoustic Formulas for Calculation of Rotating Blade Noise," *AIAA Journal*, Vol. 19, No. 9, 1981, pp. 1122–1130.

[5]Brentner, K. S., "Prediction of Helicopter Rotor Discrete Frequency Noise—A Computer Program Incorporating Realistic Blade Motions and Advanced Formulation," NASA TM-87721, Oct. 1986.

[6]Gallman, J. M., "The Validation and Application of a Rotor Acoustic Prediction Computer Program," NASA TM-101794, Jan. 1990.

[7]Spiegel, P., and Rahier, G., "Theoretical Study and Prediction of BVI Noise Including Close Interaction," American Helicopter Society–Royal Aeronautical Society International Technical Specialists Meeting on Rotorcraft Acoustics and Rotor Fluid Dynamics, Valley Forge, PA, Oct. 1991.

[8]Schultz, K. J., Lohman, D., Lieser, J. A., and Pahlke, K. D., "Aeroacoustic Calculation of Helicopter Rotors at DLR," *Fluid Dynamics Panel Symposium on Aerodynamics and Aeroacoustics of Rotorcraft*, AGARD, 1994 (Paper 29).

[9]Ianniello, S., and De Bernardis, E., "Calculation of High-Speed Noise from Helicopter Rotor Using Different Descriptions of Quadrupole Source," *Fluid Dynamics Panel Symposium on Aerodynamics and Aeroacoustics of Rotorcraft*, AGARD, 1994 (Paper 27).

[10]Brentner, K. S., and Holland, P. C., "An Efficient and Robust Method for Computing Quadrupole Noise," American Helicopter Society Second International Aeromechanics Specialists' Conf., Bridgeport, CT, 1995.

[11]Brentner, K. S., "An Efficient and Robust Method for Predicting Rotor High-Speed Impulsive Noise," AIAA Paper 96-0151, Jan. 1996.

[12]Xue, Y., and Lyrintzis, A. S., "Rotating Kirchhoff Method for Three-Dimensional Transonic Blade-Vortex Interaction Hover Noise," *AIAA Journal*, Vol. 32, No. 7, 1994, pp. 1350–1359.

[13]Baeder, J. D., Gallman, J. M., and Yu, Y. H., "A Computational Study of Aeroacoustics of Rotors in Hover," American Helicopter Society Forty-Ninth Annual Forum, St. Louis, MO, May 1993.

[14]Strawn, R. C., and Biswas, R., "Computation of Helicopter Rotor Noise in Forward Flight," *Journal of the American Helicopter Society*, Vol. 40, No. 3, 1995, pp. 66–72.

[15]Meadows, K. R., and Atkins, H. L., "Towards a Highly Accurate Implementation of the Kirchhoff Approach for Computational Aeroacoustics," *Journal of Computational Acoustics*, Vol. 4, No. 2, 1996.

[16]Özyörük, Y., and Long, L. N., "A Navier–Stokes/Kirchhoff Method for Noise Radiation from Ducted Fans," AIAA Paper 94-0462, Jan. 1994.

[17]Press, W. H., Flannery, B. P., Teukolsky, S. A., and Vetterlin, W. T., *Numerical Recipes: The Art of Scientific Computing*, Cambridge Univ. Press, Cambridge, England, UK, 1986.

[18]Farassat, F., Dunn, M. H., and Padula, S., "Advanced Turboprop Noise Prediction Based on Recent Theoretical Results," *Journal of Sound and Vibration*, Vol. 119, No. 1, 1987, pp. 53–79.

[19]Dunn, M. H., and Tarkenton, G. M., "Computational Methods in the Prediction of Advanced Subsonic and Supersonic Propeller Induced Noise–ASSPIN Users' Manual," NASA CR 4434, April 1992.

[20]Anon., Advanced Rotorcraft Technology, "Kirchhoff Code—A Versatile CAA Tool" (Yu Xue, principal investigator), NASA SBIR Phase I Final Rept., Contract NAS1-20366, June 1995.

[21]Farassat, F., and Brown, T. J., "A New Capability for Predicting Helicopter Rotor and Propeller Noise Including the Effect of Forward Motion," NASA TM X-74037, June 1977.

[22]Hanson, D. B., "Near Field Noise of High Tip Speed Propellers in Forward Flight," AIAA Paper 76-565, July 1976.

[23]Farassat, F., and Myers, M. K., "Line Source Singularity in the Wave Equation and Its Removal by Quadrupole Sources—A Supersonic Propeller Noise Problem," *Structural Acoustics, Scattering and Propagation*, edited by J. E. Ffowcs Williams, D. Lee, and A. D. Pierce, World Scientific, Singapore, 1994, pp. 29–43.

[24]Brentner, K. S., "A New Algorithm for Computing Acoustic Integrals," Fourteenth IMACS World Congress, Atlanta, GA, July 1994.

[25]Lorensen, W. E., and Cline, H. E., "Marching Cubes: A High Resolution 3D Surface Construction Algorithm," *ACM-Computer Graphics*, Vol. 21, No. 4, 1987, pp. 163–169.

[26]Wells, V., "Integrating the Acoustic Analogy for Supersonic Rotating Surfaces," AIAA Paper 89-1133, April 1989.

S. Glegg
Associate Editor